

A General Deep Reinforcement Learning Framework for Grant-Free NOMA Optimization in mURLLC

Yan Liu, *Student Member, IEEE*, Yansha Deng, *Member, IEEE*,
Hui Zhou, *Student Member, IEEE*, Maged El Kashlan, *Senior Member, IEEE*,
and Arumugam Nallanathan, *Fellow, IEEE*

Abstract

Grant-free non-orthogonal multiple access (GF-NOMA) is a potential technique to support massive Ultra-Reliable and Low-Latency Communication (mURLLC) service. However, the dynamic resource configuration in GF-NOMA systems is challenging due to the random traffics and collisions, which are unknown at the base station (BS). Meanwhile, joint consideration of the latency and reliability requirements makes the resource configuration of GF-NOMA for mURLLC more complex. To address this problem, we develop a general learning framework for signature-based GF-NOMA in mURLLC service taking into account the MA signature collision, and the UE detection as well as the data decoding procedures for the K-repetition GF scheme and the Proactive GF scheme. The goal of our learning framework is to maximize the long-term average number of successfully served users (UEs) under the latency constraint. We first perform a real-time repetition value configuration based on a double deep Q-Network (DDQN) and then propose a Cooperative Multi-Agent (CMA) learning technique based on the DQN to optimize the configuration of both the repetition values and the contention-transmission unit (CTU) numbers. Our results shown that the number of successfully served UEs achieved under the same latency constraint in our proposed learning framework is up to ten times for the K-repetition scheme, and two times for the Proactive scheme, more than those achieved in the system with fixed

Y. Liu, M. El Kashlan, and A. Nallanathan are with School of Electronic Engineering and Computer Science, Queen Mary University of London, London, UK (e-mail: {yan.liu, maged.elkashlan, a.nallanathan}@qmul.ac.uk).

Y. Deng and H. Zhou are with Department of Engineering, King's College London, London, UK (e-mail: {yansha.deng, hui.zhou}@kcl.ac.uk). (Corresponding author: Yansha Deng (e-mail: {yansha.deng}@kcl.ac.uk).)

repetition values and CTU numbers, respectively. Importantly, our general learning framework can be used to optimize the resource configuration problems in all the signature-based GF-NOMA schemes.

Index Terms

mURLLC, NOMA, grant free, deep reinforcement learning, resource configuration.

I. INTRODUCTION

As a new and dominating service class in 6th Generation (6G) networks, massive Ultra-Reliable and Low Latency Communications (mURLLC) integrates URLLC with massive access to support massive short-packet data communications in time-sensitive wireless networks with high reliability and low access latency [1], which requires a reliability-latency-scalability trade-off and mandates a principled and scalable framework accounting for the delay, reliability, and decision-making under uncertainty [2]. Concretely speaking, the Third Generation Partnership Project (3GPP) standard [3] has defined a general URLLC requirement as: $1 - 10^{-5}$ reliability within 1ms user plane latency¹ for 32 bytes. More details on the requirements of various different URLLC use cases, including smart grids, intelligent transportation systems, and process automation with reliability requirements of $1 - 10^{-3}$ to $1 - 10^{-6}$ at latency requirements between 1 ms to 100 ms, can be found in [4]. In addition, in the 6G white paper [5], it is anticipated that the device density may grow to hundred(s) of devices per cubic meter.

Current cellular network can hardly fulfill the joint massive connectivity, ultra-reliability, and low latency requirements in mURLLC service. To achieve low latency, *grant-free (GF) access* has been proposed [6] [7] as an alternative for traditional grant-based (GB) access due to its drawbacks in high latency and heavy signaling overhead [8]. Different from GB access, GF access allows a User Equipment (UE) to transmit its data to the Base Station (BS) in an arrive-and-go manner, without sending a scheduling request (SR) and obtaining a resource grant (RG) from the network [9]. To achieve high reliability, several GF schemes, including the *K-repetition* scheme and the *Proactive* scheme, have been proposed, where a pre-defined number (K) of consecutive replicas of the same packet are transmitted [10]–[13]. To achieve massive connectivity, *non-orthogonal multiple access (NOMA)* has been proposed to synergize with GF in order to deal

¹User plane latency is defined as the one-way latency from the processing of the packet at the transmitter to the successful reception of the packet, including the transmission processing time, the transmission time, and the reception processing time.

with the MA physical resource collision as shown in Fig. 1 in contention-based² GF access on orthogonal multi-access (OMA) physical resources, when two or more UEs transmit their data using the same MA physical resource [14], [15]. Here, we focus on the signature-based GF-

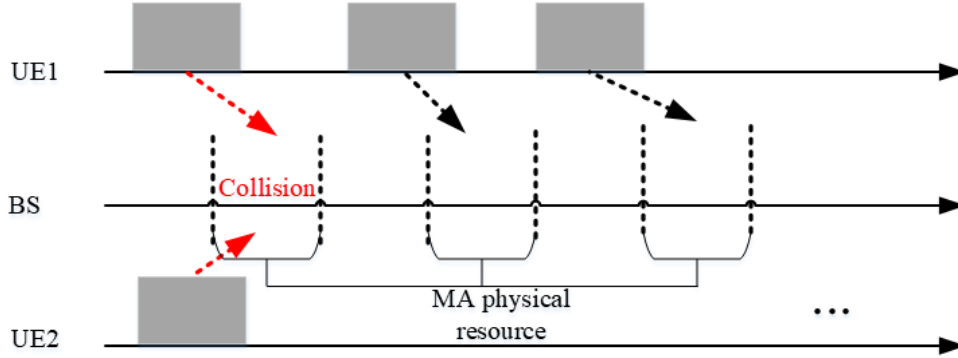


Fig. 1: Collision of MA physical resource.

NOMA, including the sparse code multiple access (SCMA), multiuser shared access (MUSA), pattern division multiple access (PDMA), and etc, where the NOMA technique allows multiple users to transmit over the same MA physical resource by employing user-specific signature patterns (e.g, codebook, pilot sequence, interleaver/mapping pattern, demodulation reference signal, power, etc.) [16]. However, when two or more UEs transmit their data using the same MA physical resource and the same MA signature, the MA signature collision occurs, and the BS cannot differentiate among different UEs and therefore cannot decode the data [14], [15].

It is important to know that the research challenges in GF-NOMA are fundamentally different from those in GB-NOMA [17], [18]. In GB scheme, the four-step random access (RA) procedure as shown in Fig. 2 is executed by the UE to request the BS to schedule dedicated resources for data transmission, where the data transmission is more likely to be successful once the random access succeeds. While in GF scheme, the data is transmitted along with the pilot in a randomly chosen MA resource, which is unknown at the BS, and can lead to new research problems including but not limited to: 1) identify the MA signature collisions due to UEs transmitting data over the same channel resource with the same MA signature; 2) blind detection of active

²Unless otherwise stated, the GF and GB access described in this work are both contention based.

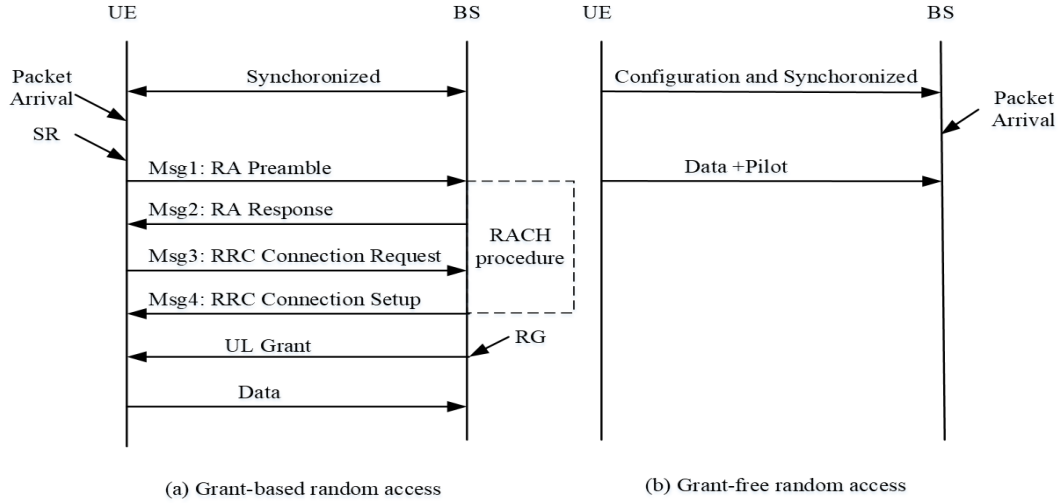


Fig. 2: Uplink transmissions for grant-based and grant-free random access.

UEs due to that the set of active users is unknown to the BS; 3) blind decoding of UEs' data with no knowledge of channels and codebooks. These new research problems make the dynamic resource configuration of GF-NOMA as one important but challenging problem to solve.

The main challenges of the dynamic resource configuration optimization of GF-NOMA include: 1) the set of active users and their respective channel conditions are unknown to the BS, which prohibits the pre-configuration and the pre-assignment of resources, including pilots/preambles, power, codebooks, repetition values, HARQ related parameters, and etc; 2) to satisfy the reliability and latency requirements simultaneously under random traffics, the optimal parameter configurations vary over different time slots, which is hard to be described by a tractable mathematical model; 3) the MA signature collision detection, and the blind UE activity detection as well as the data decoding, need to be considered, which largely impacts the resource configuration in each time slot; 4) for various signature-based NOMA schemes, a general optimization framework for GF-NOMA systems have never been established.

The above challenges can hardly be solved via traditional convex optimization method, due to the complex communication environment with the lack of tractable mathematical formulations, whereas the Machine Learning (ML) can be an potential alternative approach. In the GF-NOMA system, the BS can only observe the results of both collision detection (e.g., the number of non-collision UEs and collision MA signatures) and data decoding (e.g., the number of successful decoding UEs and failure decoding UEs) in each round trip time (RTT). This

historical information can be potentially used to facilitate the long-term optimization of future configurations. Even if one knew all the relevant statistics, tackling this problem in an exact manner would result in a Partially Observable Markov Decision Process (POMDP) with large state and action spaces, which is generally intractable. To deal with it, Reinforcement Learning (RL), can be a promising tool to deal with this complex POMDP problem of GF-NOMA resource configuration optimization, which solely relies on the self-learning of the environment interaction without deriving explicit optimization solutions based on a complex mathematical model.

In this paper, we aim to develop a general learning framework for GF-NOMA systems with mURLLC services. Our contributions can be summarized as follows:

- We develop a general learning framework for the dynamic resource configuration optimization in signature-based GF-NOMA systems, including the SCMA, MUSA, PDMA, and etc, for mURLLC services, which takes into account the MA signature collision and the UE detection as well as the data decoding procedure.
- In this framework, we aim to optimize the number of successfully transmitted UEs under the latency constraint via adaptively configuring the uplink resources for the K-repetition GF scheme and the Proactive GF scheme. The uplink GF-NOMA procedure is simulated by taking into account the random traffics, the resource selection and configuration, the transmission latency check, the collision detection, the data decoding, and the HARQ retransmission. This generated simulation environment is used for training the RL agents before deployment, and these agents will be updated according to the real traffic in practical networks in an online manner.
- We first perform the repetition values dynamic optimization, where a double Deep Q-Network (DDQN) is developed for the two GF schemes. We then extend to a more practical scenario to dynamically optimize the repetition values and MA resources configuration, where a Cooperative Multi-Agent learning based on DQN (CMA-DQN) is developed to break down the selection in high-dimensional parameters into multiple parallel sub-tasks with a number of DQN agents cooperatively being trained to produce each parameter.
- Our results shown that the number of successfully served UEs achieved under the same latency constraint in our proposed learning framework is up to ten times for the K-repetition scheme, and two times for the Proactive scheme, more than those achieved in the system with fixed repetition values and CTU numbers, respectively. In addition, our results shown

that the Proactive scheme outperforms the K-repetition scheme in terms of the number of successfully served UEs, especially under the long latency constraint of 8 ms, which is different from the analytical results without optimization in our previous work [19] with only a single packet transmission.

II. RELATED WORKS

The potential of GF-NOMA to different service is still an open research area as the research challenges of GF-NOMA have not been solved. In [20]–[22], GF-NOMA is designed empirically by directly incorporating the GF mechanism into the state-of-the-art NOMA schemes, including the SCMA, MUSA, and PDMA, which are categorized according to their specially designed spreading signatures. Most existing GF-NOMA works focused on receiver design using the compressive sensing (CS) technique. The authors in [23] proposed a message passing algorithm to solve the problem of GF-NOMA using CS-based approaches, which improves the BER performance in comparison to [24]. The authors in [25] considered a comprehensive study such that synchronization, channel estimation, user detection and data decoding are performed in one-shot. The proposed CS-based algorithm exploits the sparsity of the system in terms of user activity and multi-path fading. To the best of our knowledge, no works have focused on the optimization of the general GF-NOMA system including the MA collision detection, and UE detection as well as data decoding procedures. The major challenge comes from the fact that random user activation and non-orthogonal transmissions make the GF-NOMA hard to be mathematically modeled and optimized using traditional optimization methods.

ML has been introduced to improve the GF-NOMA systems in [26]–[28]. In [26], deep learning was used to solve a variational optimization problem for GF-NOMA. The neural network model includes encoding, user activity, signature sequence generation, and decoding. The authors then extended their work to design a generalized/unified framework for NOMA using deep multi-task learning in [27]. A deep learning-based active user detection scheme has been proposed for GF-NOMA in [28]. By feeding training data into the designed deep neural network, the proposed active user detection scheme learns the nonlinear mapping between received NOMA signal and indices of active devices. Their results shown that the trained network can handle the whole active user detection process, and achieve accurate detection of the active users. These works assumed that each UE is pre-allocated with a unique sequence, and thus collisions are not an issue. However, this assumption does not hold in massive UEs settings in mMTC, where the

collision is the bottle-neck of the GF-NOMA performance. Different from [26]–[28], we develop a general learning framework to optimize GF-NOMA systems for mURLLC service taking into account the latency constraint, the MA signature collision, and the UE detection as well as the data decoding procedures.

III. SYSTEM MODEL

We consider a single cell network consisting of a BS located at the center and a set of N UEs randomly located in an area of the plane \mathbb{R}^2 , where the UEs are in-synchronized and unaware of the status of each other. Once deployed, the UEs remain spatially static. The time is divided into short-TTIs³, and the small packets for each UE are generated according to random inter-arrival processes over the short-TTIs, which are Markovian as defined in [29] [30] and unknown to BS.

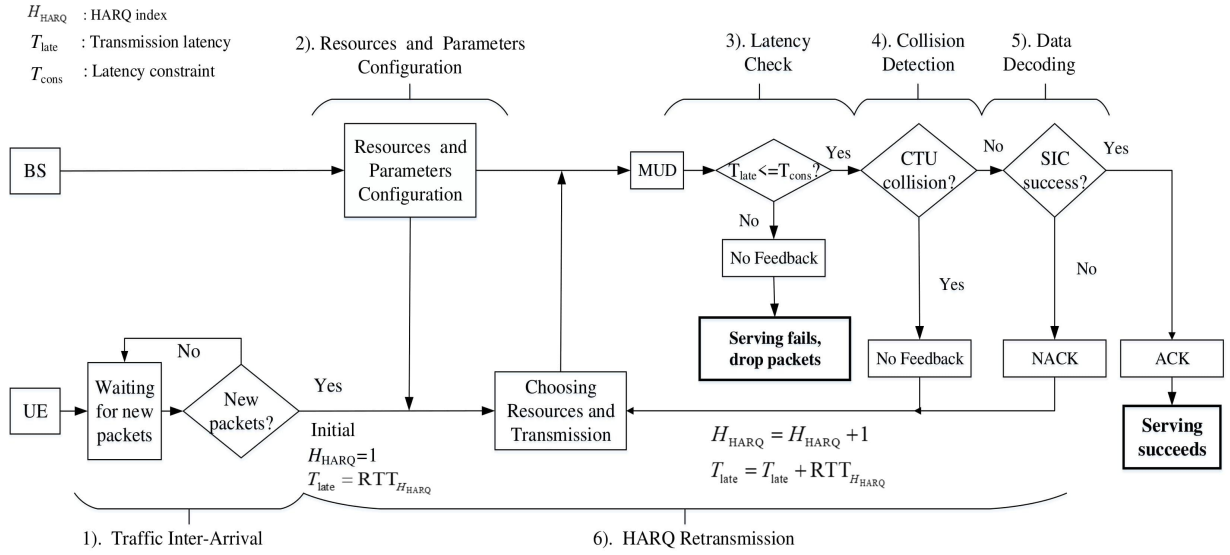


Fig. 3: Uplink GF-NOMA transmission procedure.

³5G NR introduces the concept of ‘mini-slots’ and supports a scalable numerology allowing the sub-carrier spacing (SCS) to be expanded up to 240 kHz. In contrast with the LTE slot consisting of 14 OFDM symbols per TTI, the number of OFDM symbols in 5G NR mini-slots ranges from 1 to 13 symbols, and the larger SCS decreases the length of each symbol further. Collectively, mini-slots and flexible numerology allows shorter transmission slots to meet the stringent latency requirement. In this paper, the TTI refers to a mini-slot.

A. GF-NOMA Network Model

We consider the uplink contention-based GF-NOMA over a set of preconfigured MA resources for UEs with latency constraint T_{cons} . To capture the effects of the physical radio, we consider the standard power-law path-loss model with the path-loss attenuation $r^{-\eta}$, where r is the Euclidean distance between the UE and the BS and η is the path-loss attenuation factor. In addition, we consider a Rayleigh flat-fading environment, where the channel power gains h are exponentially distributed (i.i.d.) random variables with unit mean. Fig. 3 presents the uplink GF-NOMA procedure following the 3GPP standard [9], [12], [13], [31], [32], which includes: 1) traffic inter-arrival, 2) resources and parameters configuration, 3) latency check; 4) collision detection, 5) data decoding, and 6) Hybrid Automatic Repeat reQuest (HARQ) retransmissions. These six stages are explained in the following six subsections to introduce the system model.

1) *Traffic Inter-Arrival*: We consider a bursty traffic scenario, where massive UEs are recovered due to an emergency event, e.g., earthquake alarm and fire alarms [30], [33]. Each UE would be activated at any time τ , according to a time limited Beta probability density function given as [30, Section 6.1.1]

$$p(\tau) = \frac{\tau^{\alpha-1}(T-\tau)^{\beta-1}}{T^{\alpha+\beta-1}\text{Beta}(\alpha, \beta)}, \quad (1)$$

where T is the total time of the bursty traffic and Beta (α, β) is the Beta function with the constant parameters α and β [34].

Due to the nature of slotted-Aloha, a UE can only transmit at the beginning of a RTT as shown in Fig. 4 and Fig. 5, which means that the newly activated UEs executing transmission come from those who received an packet within the interval between with the last RTT period (τ^{i-1}, τ^i) . The traffic instantaneous rate in packets in a period is described by a function $p(\tau)$, so that the packets arrival rate in the i th RTT is given by

$$\mu^i = \int_{\tau_{i-1}}^{\tau_i} p(\tau) d\tau. \quad (2)$$

2) *Resources and Parameters Configuration*: The UEs are configured by radio resource control (RRC) signaling and L1 signaling prior to the GF access (as Type 2 GF [35]), with MA resources, repetition values, and HARQ related parameters, etc.

a) *Repetition values*: We consider two GF schemes, which are the K-repetition scheme and the Proactive scheme in this work as shown in Fig. 4 and Fig. 5, respectively. The repetition values for K-repetition scheme K_{Krep}^t and for Proactive scheme K_{Proa}^t are configured at the beginning

of each RTT in order to be adapted to guarantee the reliability and latency requirements based on the random traffic.

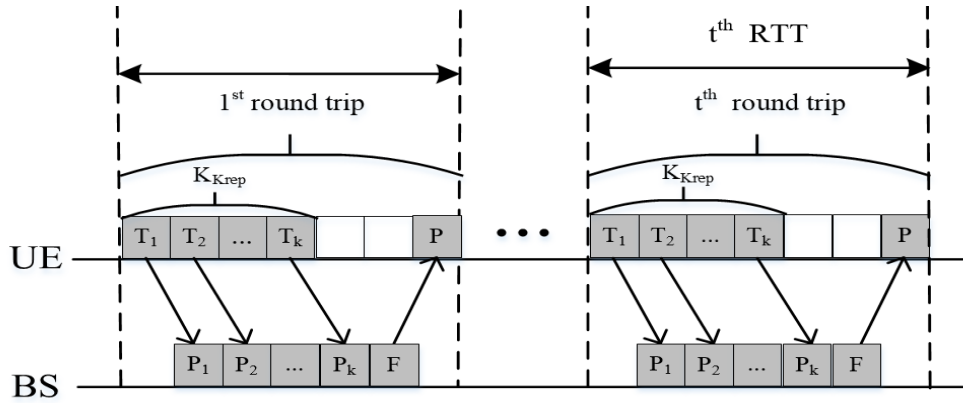


Fig. 4: K-repetition GF transmission

- **K-repetition scheme:** The K-repetition scheme is illustrated in Fig. 4, where the UE is configured to autonomously transmit the same packet for K_{Krep}^t repetitions in consecutive TTIs. The BS decodes each repetition independently and the transmission in one RTT is successful when at least one repetition succeeds. After processing all the received K_{Krep}^T repetitions, the BS transmits the ACK/NACK back to the UE.

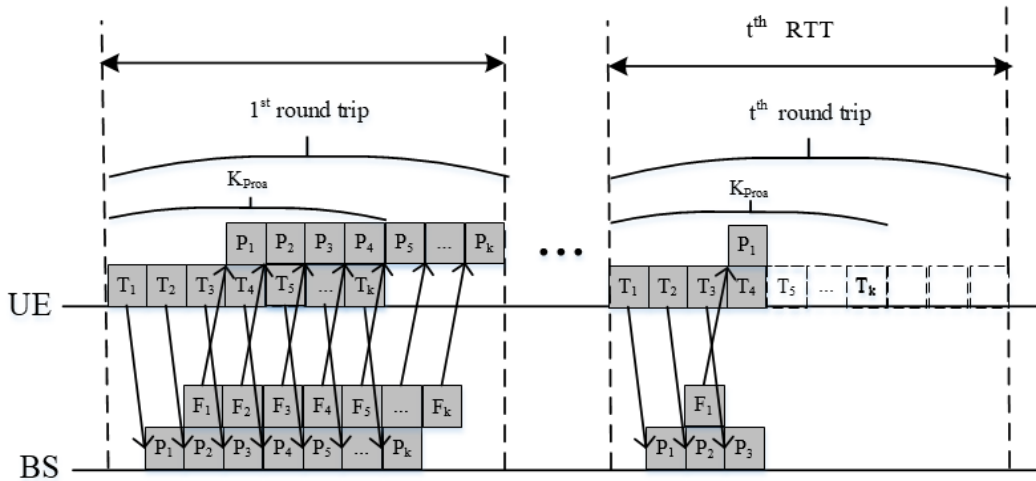


Fig. 5: Proactive GF transmission

- **Proactive scheme:** The Proactive scheme is illustrated in Fig. 5. Similar to the K-repetition scheme, the UE is configured to repeat the transmission for a maximum number of K_{Proa}^t

repetitions, but can receive the feedback after each repetition. This allows the UE to terminate repetitions earlier once receiving the ACK.

Considering the small packets of mURLLC traffic, we set the packet transmission time as one TTI. The BS feedback time and the BS (UE) processing time are also assumed to be one TTI following our previous work [19]. Once the repetition value is configured, the duration of one RTT is known to the UEs and the BS, which is given as

$$T_{\text{RTT}}^t = (K^t + 3)\text{TTIs}, \quad (3)$$

with $K^t = K_{\text{Krep}}^t$ or $K^t = K_{\text{Proa}}^t$ for the K-repetition scheme and the Proactive scheme, respectively.

b) MA resources: A *contention-transmission unit* (CTU) as shown in Fig. 6 is defined as the basic MA resource, where each CTU may comprise of a MA physical resource and a MA signature [7] [15] [36]. The MA physical resources represent a set of time-frequency resource

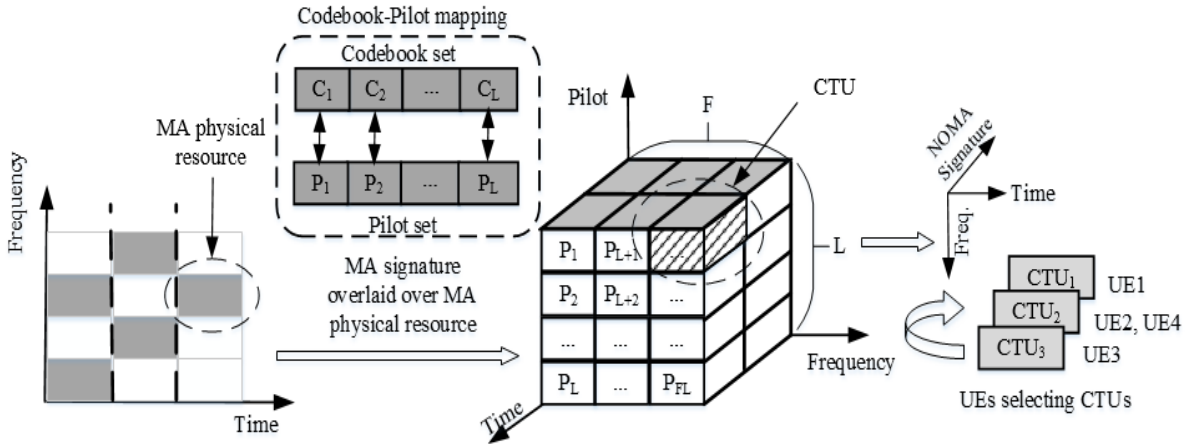


Fig. 6: GF-NOMA resource

blocks (RBs). The MA signatures represent a set of pilot sequences for channel estimation and/or UE activity detection, and a set of codebooks for robust data transmission and interference whitening, etc. Without loss of generality, in one TTI, we consider F orthogonal RBs and each RB is overlaid with L unique codebook-pilot⁴ pairs [14] [38]. Thus, at the beginning of each

⁴A one-to-one mapping or a many-to-one mapping between the pilot sequences and codebooks can be predefined. Since it has been verified in [20] that the performance loss due to codebook collision is negligible for a real system, we focus on the pilot sequence collision and consider the one-to-one mapping in our work like [14] [37].

RTT, the BS configures a resource pool of $C^t = F \times L$ unique CTUs, and each UE randomly choose one CTU from the pool to transmit in this RTT.

3) *Latency Check:* The HARQ index H_{HARQ} is included in the pilot sequence and can be detected by the BS. At the beginning of each RTT, the HARQ index and the transmission latency T_{late} will be updated as shown in Fig. 3. For example, for the initial RTT with initial K^1 , $H_{HARQ} = 1$ and $T_{late} = RTT_{H_{HARQ}=1}$, where $RTT_{H_{HARQ}}$ is calculated by using (3). After this round time trip transmission, the BS optimizes a K^2 based on the observation of the reception and configures it to the UE for the next RTT. Then the UE updates its $H_{HARQ} = 2$ and calculated $RTT_{H_{HARQ}=2}$ by using (3) with K^2 , and consequently, the transmission latency T_{late} is updated as $T_{late} = RTT_{H_{HARQ}=1} + RTT_{H_{HARQ}=2}$. When $T_{late} > T_{cons}$, the UE fails to be served and the packets will be dropped. Note that the HARQ index, as well as the transmission latency, will be updated at the beginning of each RTT instead of at the end of each RTT due to that we consider the user plane latency in this work, which has been explained in footnote 1. That is to say, from the UE perspective, when the UE executes this RTT, it will check transmission results after finishing the RTT. Thus, the duration of this RTT should be included when calculating the UE transmission latency.

4) *Collision Detection:* At each RTT, each active UE transmits its packets to the BS by randomly choosing a CTU. The BS can detect the UEs that have chosen different CTUs. However, if multiple UEs choose the same CTU, the BS cannot differentiate the these UEs and therefore cannot decode the data. We categorize the CTUs into three types. An *idle* CTU is a CTU which has not been chosen by any UE. A *singleton* CTU is a CTU chosen by only one UE, and a *collision* CTU is a CTU chosen by two or more UEs [14]. One example is illustrated in Fig. 7, where UE 1 and UE 5 performed the GF-NOMA transmissions by choosing the unique CTU 6 and CTU 5, respectively, where CTU 6 and 5 are the singleton CTUs. The CTU 3 is the idle CTU. UE 4 and UE 7 have chosen the CTU 1, UE 2 and UE 3 have chosen the CTU 2, and UE 6 and UE 8 have chosen the CTU 4, where CTU 1, 2 and 4 are the collision CTUs. At the t th RTT, we denote the set of singleton CTUs as \mathcal{C}_{sc}^t , the set of idle CTUs as \mathcal{C}_{ic}^t , and the set of collision CTUs as \mathcal{C}_{cc}^t .

5) *GF-NOMA Data Decoding:* After detecting UEs that have chosen the singleton CTUs (e.g., UE 1 and 5 in Fig. 7), the BS applies successive interference cancellation (SIC) technique to decode the data of these UEs. When decoding, the BS treats the UEs that transmit in the same RB as the interference as shown in Fig. 7, and the UEs that transmit in different RBs do not

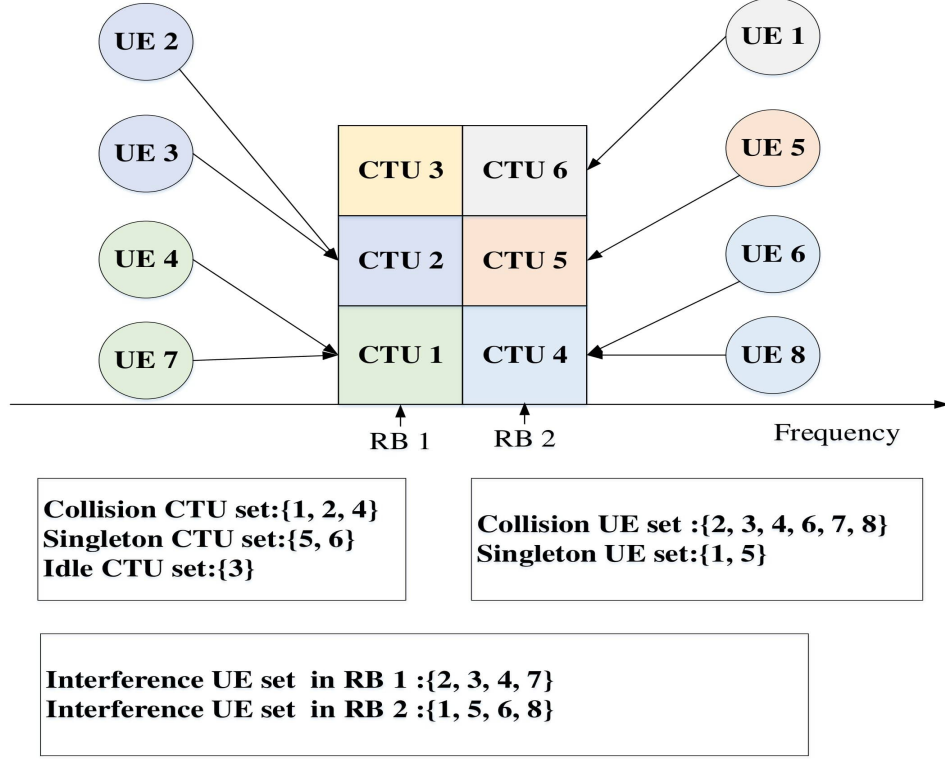


Fig. 7: Collision detection case of a network with $L=2$ RBs, $C = 6$ CTUs and $N = 8$ UEs.

interfere with each other due to the orthogonality. In each iterative stage of SIC decoding, the CTU with the strongest received power is decoded by treating the received powers of other CTUs over the same RB as the interference. Each iterative stage of SIC decoding is successful when the signal-to-interference-plus-noise ratio (SINR) in that stage is larger than the SINR threshold. If the received signal is decoded successfully, the decoded signal is subtracted from the received signal⁵. Thus, in the k th repetition of the t th RTT, the s th SIC decoding is successful if

$$\text{SINR}_{f,s}^t(k) = \frac{P h_{s,k} r_s^{-\eta}}{\sum_{m=s+1}^{N_{f,sc}^t(k)} P_m h_{m,k} r_m^{-\eta} + \sum_{n' \in \mathcal{N}_{f,cc}^t(k)} P_{n'} h_{n',k} r_{n'}^{-\eta} + \sigma^2} \geq \gamma_{th}, \quad (4)$$

where P is the transmission power, $\mathcal{N}_{f,sc}^t$ is the set of devices that have chosen the singleton CTUs over the f th RB, $\mathcal{N}_{f,cc}^t$ is the set of devices that have chosen the collision CTUs over the f th RB, σ^2 is the noise power, and γ_{th} is the SINR threshold.

⁵We assume perfect SIC the same as [14], with no error propagation between iterations.

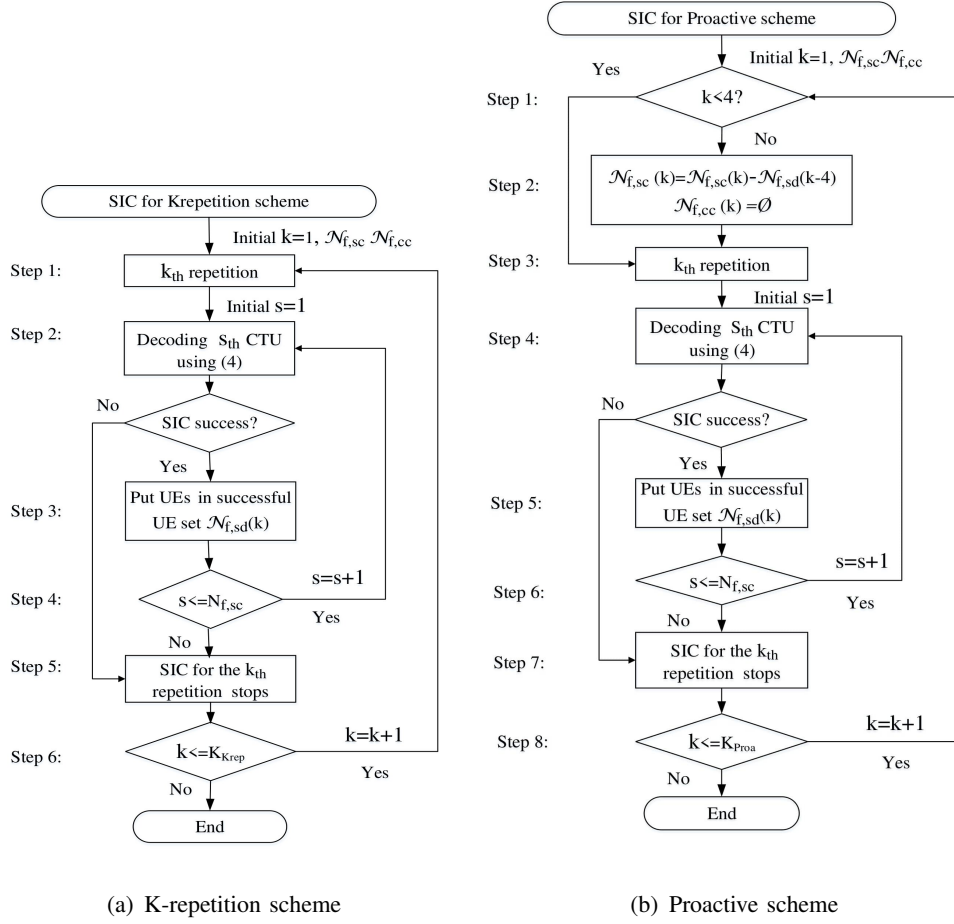


Fig. 8: SIC decoding procedure for each GF scheme.

The SIC procedure stops when one stage of the SIC fails or when there are no more signals to decode. The SIC decoding procedure for each GF scheme is given in Fig. 8 with the details described in the following.

i) K-repetition scheme: For the K-repetition scheme as shown in Fig. 4, the successful decoding event occurs at least one repetition decoding succeeds. Thus, the SIC decoding procedure follows:

- Step 1: Start the k th repetition with the initial $k = 1$, $\mathcal{N}_{f,sc}^t$ and $\mathcal{N}_{f,cc}^t$;
- Step 2: Decode the s th CTU with the initial $s = 1$ using (4);
- Step 3: If the s th CTU is successfully decoded, put the decoded UE in set $\mathcal{N}_{f,sd}^t(k)$ and go to Step 4, otherwise go to Step 5;
- Step 4: If $s \leq N_{f,sc}^t$, do $s = s + 1$, go to Step 2, otherwise go to Step 5;
- Step 5: SIC for the k th repetition stops;

- Step 6: If $k \leq K_{\text{Krep}}$, do $k = k + 1$, go to Step 1, otherwise go to the end.

ii) Proactive scheme: For the Proactive scheme as shown in Fig. 5, the successful decoding event occurs once the repetition decoding succeeds. The successfully decoded UEs will not transmit in the remaining repetitions to reduce interference to other UEs. It should be noted that the ACK/NACK feedback can only be received after 3TTIs, which means the ACK feedback of the k th successful repetition can be received by the UE in the $(k + 3)$ th repetition and the UE stops transmission from the $(k + 4)$ th repetition. In addition, the BS does not send any ACK/NACK feedback to the collision UEs. The collision UEs in the k th repetition that do not receive feedback at the pre-defined timing after the UEs sent the packet (e.g., after 3TTIs) will not transmit in the remaining repetitions to reduce interference to other UEs.

- Step 1: Initialize $k = 1$, $\mathcal{N}_{f,sc}^t$ and $\mathcal{N}_{f,cc}^t$. If $k < 4$, go to Step 3, otherwise go to Step 2;
- Step 2: Update the $\mathcal{N}_{f,sc}^t(k) = \mathcal{N}_{f,sc}^t(k) - \mathcal{N}_{f,sc}^t(k - 4)$ and $\mathcal{N}_{f,cc}^t(k) = \emptyset$;
- Step 3: Start the k th repetition with k , $\mathcal{N}_{f,sc}^t(k)$ and $\mathcal{N}_{f,cc}^t(k)$;
- Step 4: Decode the s th CTU with initial $s = 1$ using (4);
- Step 5: If the s th CTU is successfully decoded, put the decoded UE in set $\mathcal{N}_{f,sd}^t(k)$ and go to Step 6, otherwise go to Step 7;
- Step 6: If $s \leq N_{f,sc}^t$, do $s = s + 1$, go to Step 4, otherwise go to Step 7;
- Step 7: SIC for the k th repetition stops;
- Step 8: If $k \leq K_{\text{Pro}}$, do $k = k + 1$, go to Step 1, otherwise go to the end.

Finally, the set $\mathcal{N}_{f,sd}^t = \bigcup_{k=1}^{K_{\text{Krep}}} (\mathcal{N}_{f,sd}^t(k))$ is the successfully decoded UEs over the f th RB and

$\mathcal{N}_{sd}^t = \bigcup_{f=1}^{F^t} (\mathcal{N}_{f,sd}^t)$ is the successfully decoded UEs in the t th RTT.

6) *GF-NOMA Retransmissions (HARQ):* We introduce the GF-NOMA HARQ retransmissions to achieve high reliability performance. However, due to the latency constraint, the HARQ retransmission times is limited as shown in Fig. 3. The UE determines a re-transmission or not based on the following two different scenarios.

i) when the UE receives an ACK from the BS, it means that the BS successfully detected the UE (i.e., the UE choosing the singleton CTUs) and decoded the UE's data (i.e., SIC succeeds), no further re-transmission is needed;

ii) when the UE receives a NACK from the BS, it means that the BS successfully detected the UE but failed to decode the UE's data (i.e., SIC fails). Otherwise, when the UE does not receive any feedback at the pre-defined timing after the UE sent the packet (e.g., at the end of

one RTT), it means the BS failed to identify the UE, the UE determines whether to retransmit or not based on the transmission latency check as shown in Fig. 3.

B. Problem Formulation

We focus the uplink contention-based GF-NOMA procedure over a set of preconfigured MA resources for UEs with latency constraint T_{cons} under two GF schemes. Each UE has only two possible states, either *inactive* or *active*, while a UE with small data packets to be transmitted is in the active state. Once activated in a given RTT t , a UE executes the GF-NOMA procedure, where the UE randomly chooses one of the preconfigured C^t CTUs to transmit its packets for K_{Krep}^t times or $k_{\text{Proa}}^t \leq K_{\text{Proa}}^t$ times under the K-repetition scheme and the Proactive scheme, respectively. During this RTT, the GF-NOMA fails if: (i) a CTU collision occurs when two or more UEs choose the same CTU (i.e., UE detection fails); or (ii) the SIC decoding fails (i.e., data decoding fails). Once failed, UEs decides whether to retransmit in the following RTT or not based on the transmission latency check. When $T_{\text{late}} > T_{\text{cons}}$, the UE fails to be served and its packets will be dropped. It is obvious that 1) increasing the repetition values K^t could improve the GF-NOMA success probability, but results in an increasing latency; 2) increasing CTU numbers C^t could improve the UE detection success probability, but it results in low resource utilization efficiency.

Thus, it is necessary to tackle the problem of optimizing the GF-NOMA configuration defined by parameters $A^t = \{K^t, C^t\}$ ⁶ for each RTT t under both the K-repetition scheme and the Proactive scheme, where K^t is the repetition value and C^t is the number of CTUs. At the beginning of each RTT t , the decision is made by the BS according to the transmission receptions $U^{t'}$ for all prior RTTs $t' = 1, \dots, t-1$, consisting of the following variables: the number of the collision CTUs $V_{cc}^{t'}$, the number of the idle CTUs $V_{ic}^{t'}$, the number of the singleton CTUs $V_{sc}^{t'}$, the number of UEs that have been successfully detected and decoded under the latency constraint $V_{sd}^{t'}$, and the number of UEs that have been successfully detected but not successfully decoded $V_{ud}^{t'}$. We denote $H^t = \{O^1, O^2, \dots, O^{t-1}\}$ with $O^{t-1} = \{U^{t-1}, A^{t-1}\}$ as the observation in each RTT t including histories of all such measurements and past actions.

⁶According to the UE detection and data decoding procedure described in Section II.A, for the same CTU number C^t , a large RB number F^t leads to fewer UEs in each RB, which increases the data decoding success probability. That is to say, the larger RB number, the better. Thus, we fix the RB number $F = 4$ in this work to optimize the CTU number.

At each RRT t , the BS aims at maximizing a long-term objective R_t (reward) related to the average number of UEs that have successfully send data under the latency constraint $V_{sd}^{t'}$ with respect to the stochastic policy π that maps the current observation history O^t to the probabilities of selecting each possible parameters in A^t . This optimization problem (P1) can be formulated as:

$$(P1 :) \max_{\pi(A^t|O^t)} \sum_{k=t}^{\infty} \gamma^{k-t} \mathbb{E}_{\pi}[V_{sd}^k] \quad (5)$$

$$s.t. \quad T_{\text{late}} \leq T_{\text{cons}}, \quad (6)$$

where $\gamma \in [0, 1)$ is the discount factor for the performance accrued in the future RTTs, and $\gamma = 0$ means that the agent just concerns the immediate reward.

Since the dynamics of the GF-NOMA system is Markovian over the continuous RRTs, this is a Partially Observable Markov Decision Process (POMDP) problem which is generally intractable. Here, the partial observation refers to that a BS can not fully know all the information of the communication environment, including, but not limited to, the channel conditions, the UE transmission latency, the random collision process, and the traffic statistics. Furthermore, the traditional optimization methods may need global information to achieve the optimal solution, which not only increases the overhead of signal transmission, but also increase the computation complexity, or even hardly deal with. Approximate solutions will be discussed in Section IV.

IV. DEEP REINFORCEMENT LEARNING-BASED GF-NOMA RESOURCE CONFIGURATION

The deep reinforcement learning (DRL) has been regarded as a powerful tool to address complex dynamic control problems in POMDP with large state spaces [39], [40], since it has the potential to accurately approximate the desired value function via the combination of DNN structures. In this section, we proposed a Deep Q-network (DQN) based algorithm for tackling the formulated problem P1. To evaluate the capability of DQN in GF-NOMA, we first consider the dynamic configuration of repetition value K^t with fixed CTU numbers C^t , where the DQN agent dynamically configures the K^t at the beginning of each RTT for K-repetition and Proactive GF schemes. We then propose a cooperative multi-agent learning technique based on the DQN to optimize the configuration of both repetition value K^t and CTU numbers C^t simultaneously, which breaks down the selection in high-dimensional action space into multiple parallel sub-tasks.

A. Deep reinforcement learning-based single-parameter configuration

1) *Reinforcement learning framework*: To optimize the number of successfully served UEs under the latency constraint in GF-NOMA schemes, we consider a RL-agent deployed at the BS to interact with the environment in order to choose appropriate actions progressively leading to the optimization goal. We define $s \in \mathcal{S}$, $a \in \mathcal{A}$, and $r \in \mathcal{R}$ as any state, action, and reward from their corresponding sets, respectively. The RL-agent first observes the current state S^t corresponding to a set of previous observations ($O^t = \{U^{t-1}, U^{t-2}, \dots, U^1\}$) in order to select an specific action $A^t \in \mathcal{A}(S^t)$. Here, the action A^t represents the repetition values K^t in the t th RTT $A^t = K^t$ in this single-parameter configuration scenario and the S^t is a set of indices mapping to the current observed information $U^{t-1} = [V_{cc}^{t-1}, V_{ic}^{t-1}, V_{sc}^{t-1}, V_{sd}^{t-1}, V_{ud}^{t-1}]$. With the knowledge of the state S^T , the RL-agent chooses an action A^t from the set \mathcal{A} . Once an action A^t is performed, the RL-agent transits to a new observed state S^{t+1} and receives a corresponding reward R^{t+1} as the feedback from the environment, which is designed based on the new observed state S^{t+1} and guides the agent to achieve the optimization goal. As the optimization goal is to maximize the number of the successfully served UEs under the latency constraint, we define the reward R^{t+1} as

$$R^{t+1} = V_{sd}^t, \quad (7)$$

where V_{sd}^t is the observed number of successfully served UEs under the latency constraint T_{cons} .

To select an action A^t based on the current state S^t , a mapping policy $\pi(a|s)$ learned from a state-action value function $Q(s, a)$ is needed to facilitate the action selection process, which indicates probability distribution of actions with given states. Accordingly, our objective is to find an optimal value function $Q^*(s, a)$ with optimal policy $\pi^*(a|s)$. At each RTT, $Q(s, a)$ is updated based on the received reward by following

$$Q(S^t, A^t) = Q(S^t, A^t) + \lambda[R^{t+1} + \gamma \max_{a \in \mathcal{A}} Q(S^{t+1}, a) - Q(S^t, A^t)], \quad (8)$$

where λ is a constant learning rate reflecting how fast the model is adapted to the problem, $\gamma \in [0, 1)$ is the discount rate that determines how current rewards affects the value function updating. After enough iterations, the BS can learn the optimal policy that maximizes the long-term rewards.

2) *Deep Q-network*: When the state and action spaces are large, the RL algorithm becomes expensive in terms of memory and computation complexity, which is difficult to converge to the

optimal solution. To overcome this problem, DQN is proposed in [40], where the Q-learning is combined with Deep Neural Network (DNN) to train a sufficiently accurate state-action value function for the problems with high dimensional state space. Furthermore, the DQN algorithm utilizes the experience replay technique to enhance the convergence performance of RL. When updating the DQN algorithm, mini-batch samples are selected randomly from the experience memory as the input of the neural network, which breaks down the correlation among the training samples. In addition, through averaging the selected samples, the distribution of training samples can be smoothed, which avoids the training divergence.

In DQN algorithm, the action-state value function $Q(s,a)$ is parameterized via a function $Q(s,a,\theta)$, where θ represents the weights matrix of a multiple layers DNN. We consider the conventional fully-connected DNN, where the neurons between two adjacent layers are fully pairwise connected. The variables in the state S^t is fed in to the DNN as the input; the Rectifier Linear Units (ReLUs) are adopted as intermediate hidden layers by utilizing the function $f(x) = \max(0, x)$; while the output layer is consisted of linear units, which are in one-to-one correspondence with all available actions in \mathcal{A} .

To achieve exploitation, the forward propagation of Q-function $Q(s,a,\theta)$ is performed according to the observed state S^t . The online update of weights matrix θ is carried out along each training episode to avoid the complexities of eligibility traces, where a double deep Q-learning (DDQN) training principle [41] is applied to reduce the overestimations of value function (i.e., sub-optimal actions obtain higher values than the optimal action). Accordingly, learning takes place over multiple training episodes, where each episode consists of several RTT periods. In each RTT, the parameter θ of the Q-function approximator $Q(s,a,\theta)$ is updated using RMSProp optimizer [42] as

$$\theta^{t+1} = \theta^t - \lambda_{\text{RMS}} \nabla L^{\text{DDQN}}(\theta^t) \quad (9)$$

where $\lambda_{\text{RMS}} \in (0, 1]$ is RMSProp learning rate, $\nabla L^{\text{DDQN}}(\theta^t)$ is the gradient of the loss function $L^{\text{DDQN}}(\theta^t)$ used to train the state-action value function. The gradient of the loss function is defined as

$$\nabla L^{\text{DDQN}}(\theta^t) = \mathbb{E}_{S^i, A^i, R^{i+1}, S^{i+1}} [(R^{i+1} + \gamma \max_{a \in \mathcal{A}} Q(S^{i+1}, a, \bar{\theta}^t) - Q(S^i, A^i, \theta^t)) \nabla_{\theta} Q(S^i, A^i, \theta^t)]. \quad (10)$$

We consider the application of minibatch training, instead of a single sample, to update the value function $Q(s,a,\theta)$, which improves the convergent reliability of value function $Q(s,a,\theta)$.

Therefore, the expectation is taken over the minibatch, which are randomly selected from previous samples $(S_i, A_i, S_{i+1}, R_{i+1})$ for $i \in \{t - M_r, \dots, t\}$ with M_r being the replay memory size [39]. When $t - M_r$ is negative, it represents to include samples from the previous episode. Furthermore, $\bar{\theta}^t$ is the target Q-network in DDQN that is used to estimate the future value of the Q-function in the update rule, and $\bar{\theta}^t$ is periodically copied from the current value θ^t and kept unchanged for several episodes.

Through calculating the expectation of the selected previous samples in minibatch and updating the θ^t by (9), the DQN value function $Q(s, a, \theta)$ can be obtained. The detailed DQN algorithm is presented in Algorithm 1.

B. Cooperative Multi-Agent Learning-based multi-parameter optimization

In practice, not only the repetition values but also the CTU numbers, influence reliability-latency performance in GF-NOMA. Fixed CTU numbers cannot adapt to the dynamics of the random traffic, which may violate the stringent latency requirement or lead to low resource efficiency. Thus, we study the problem (P1) of jointly optimizing the resource configuration with parameters $A^t = \{K^t, C^t\}$ to improve the network performance. The learning algorithm provided in Sec. III.A is model-free, and thus the learning structure can be extended in this multi-parameter scenario.

Due to the high capability of DQN to handle problems with massive state spaces, we consider to improve the state spaces with more observed information to support the optimization of RL-agent. Therefore, we define the current state S^t , to include information about the last M_o RTTs $(U^{t-1}, U^{t-2}, U^{t-3}, \dots, U^{t-M_o})$, which enables the RL-agent to estimate the trend of traffic. Similar to the state spaces, the available action spaces also exponentially increases with the increment of the adjustable parameter configurations in GF-NOMA. The total number of available actions corresponds to the possible combinations of all parameter configurations

Although the GF-NOMA configuration is managed by a central BS, breaking down the control of multiple parameters as multiple sub-tasks is sufficient to deal with the problems with unsolvable action space, which are cooperatively handled by independent Q-agents. As shown in Fig. 9, we consider multiple DQN agents that are centralized at the BS following the same structure of value function approximator as Sec. III.A. Each DQN agent controls their own action variable, namely K^t or C^t , and receives a common reward to guarantee the objective in P1 cooperatively.

Algorithm 1: DQN Based GF-NOMA Uplink Resource Configuration

Input: The set of repetition values in each RTT K and Operation Iteration I .

```

1 Algorithm hyperparameters: learning rate  $\lambda_{RMS} \in (0, 1]$ , discount rate  $\gamma \in [0, 1]$ ,
    $\epsilon$ -greedy rate  $\epsilon \in (0, 1]$ , target network update frequency  $K$ ;
2 Initialization of replay memory  $M$  to capacity  $D$ , the state-action value function
    $Q(S, A, \theta)$ , the parameters of primary Q-network  $\theta$ , and the target Q-network  $\bar{\theta}$ ;
3 for  $Iteration \leftarrow 1$  to  $I$  do
4   Initialization of  $S^1$  by executing a random action  $A^0$  and bursty traffic arrival rate
      $\mu^0 = 0$ ;
5   for  $t \leftarrow 1$  to  $T$  do
6     Update  $\mu^0$  using Eq. (2);
7     if  $p_\epsilon < \epsilon$  Then select a random action  $A^t$  from  $\mathcal{A}$ ;
8     else select  $A^t = \arg \max_{a \in \mathcal{A}} Q(S^t, a, \theta)$ . The BS broadcasts  $K(A^t)$  and backlogged
       UEs attempt communication in the  $t$ th RTT;
9     The BS observes state  $S^{t+1}$ , and calculate the related reward  $R^{t+1}$  using Eq. (7);
10    Store transition  $(S^t, A^t, R^{t+1}, S^{t+1})$  in replay memory  $M$ ;
11    Sample random minibatch of transitions  $(S^t, A^t, R^{t+1}, S^{t+1})$  from replay memory
       $M$ 
12    Perform a gradient descent step and update parameters for  $Q(s, a, \theta)$  using Eq.
      (10);
13    Update the parameter  $\bar{\theta} = \theta$  of the target Q-network every  $J$  steps.
14  end
15 end

```

However, the common reward design also poses challenge on the evaluation of each action, because the individual effect of specific action is deeply hidden in the effects of the actions taken by all other DQN agents. For instance, a positive action taken by a agent can receive a misleading low reward due to other DQN agents' negative actions. Fortunately, in GF-NOMA scenario, all DQN agents are centralized at the BS and share full information among each other. Accordingly, we include the action selection histories of each DQN agent as part of state function, and hence, the agents are able to learn the relationship between the common reward

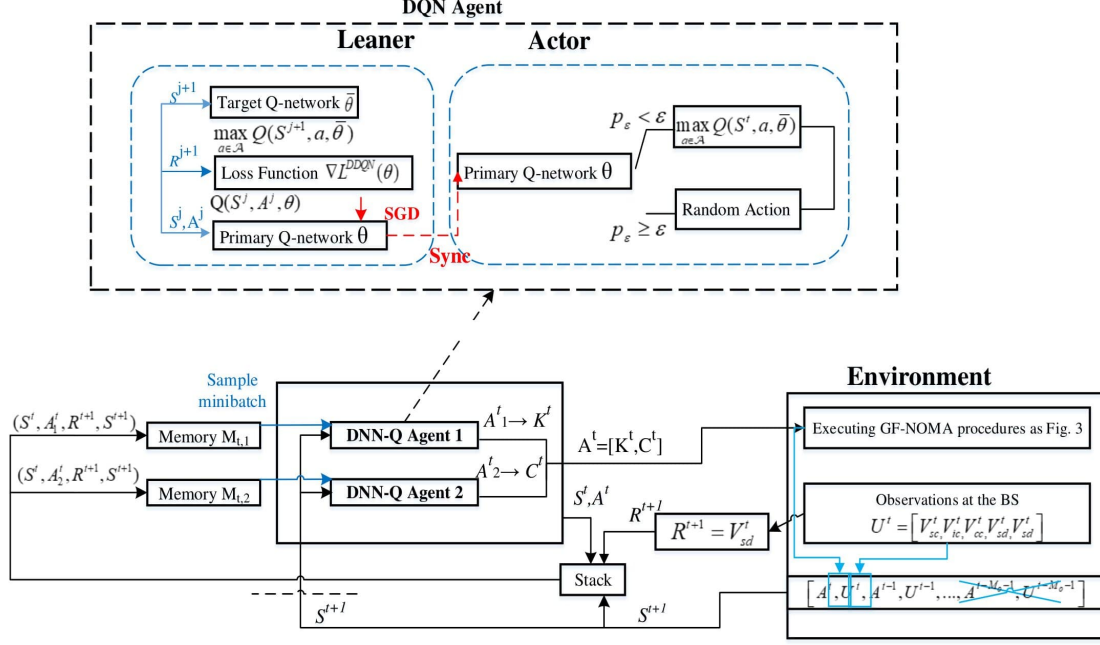


Fig. 9: The CMA-DQN agents and environment interaction in the POMDP.

and different combinations of actions. To do so, we define state variable S^t as

$$S^t = [A^{t-1}, U^{t-1}, A^{t-2}, U^{t-2}, \dots, A^{t-M_o}, U^{t-M_o}], \quad (11)$$

where M_o is the number of stored observations, A^{t-1} is the set of selected action of each DQN agent in the $(t-1)$ th TTI corresponding to K^{t-1} , and C^{t-1} , and U^{t-1} is the set of observed transmission receptions.

In each RTT, the k th agent update the parameters θ_k of the value function $Q(s, a_k, \theta_k)$ using RMSProp optimizer following Eq. (9). The learning algorithm can be implemented following Algorithm 1. Different from the GF NOMA single-parameter configuration scenario in Section III.A, it is required to initialize two primary networks θ_k , target networks $\bar{\theta}_k$ and the replay memories M_k for each DQN agent. In step 10 of Algorithm 1, each agent stores their own current transactions in memory separately. In step 11 and 12 of Algorithm 1, the minibatch of transaction should separately be sampled from individual memory to train the corresponding DQN agent.

V. SIMULATION RESULTS

In this section, we examine the effectiveness of our proposed GF-NOMA schemes with DQN algorithm via simulation. We adopt the standard network parameters listed in Table I following [43], and hyperparameters for the DQN learning algorithm are listed in Table II. All testing

TABLE II: Simulation Parameters

Parameters	Value	Parameters	Value
Path-loss exponent η	4	Noise power σ^2	-132 dBm
Transmission power P	23 dBm	The received SINR threshold γ_{th}	-10 dB
Duration of traffic T	2 s	The set of the repetition value	{1, 2, 4, 6, 8}
The set of the CTU number	{12, 24, 36, 48}	Latency constraint	2 ms and 8 ms
Bursty traffic parameter Beta(α, β)	(2, 4)	The number of bursty UEs N	20000
Cell radius	10 km	Duration of one TTI	0.125 ms

TABLE III: Learning Hyperparameters

Hyperparameters	Value	Hyperparameters	Value
Learning rate λ_{RMS}	0.0001	Minimum exploration rate ϵ	0.1
Discount rate γ	0.5	Minibatch size	32
Replay Memory	10000	Target Q-network update frequency	1000

performance results are obtained by averaging over 1000 episodes. The BS is located at the center of a circular area with a 10 km radius, and the UEs are randomly located within the cell. Unless otherwise stated, we consider the number of bursty UEs to be $N = 20000$. The DQN is set with two hidden layers, each with 128 ReLU units. In the following, we present our simulation results of the single-repetition configuration and the multi-parameter configuration in Section V-A and Section V-B, respectively. The single-repetition configuration is optimized under the latency constraint $T_{\text{cons}} = 2$ ms and the multi-parameter configuration is optimized under the latency constraint $T_{\text{cons}} = 8$ ms, respectively.

A. Single-repetition configuration

In the single-repetition configuration scenario, we set the number of CTU as $C = 48$. Throughout epoch, each UE has a periodical a bursty traffic profile (i.e., the time limited Beta profile defined in (1) with parameters (2, 4) that has a peak around the 4000th TTI.

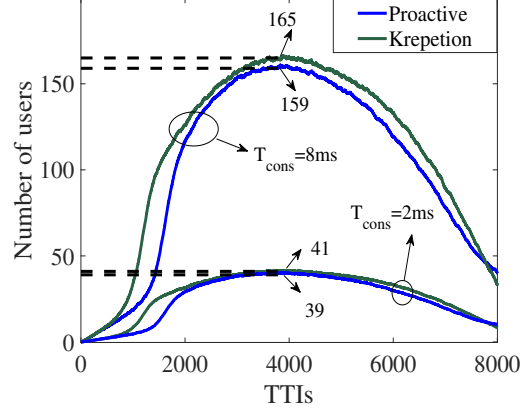


Fig. 10: Backlog traffic in each TTI under latency constraint $T_{\text{cons}} = 2$ ms and $T_{\text{cons}} = 8$ ms, respectively.

Fig. 10 plots the backlog traffic in each TTI under latency constraint $T_{\text{cons}} = 2$ ms and $T_{\text{cons}} = 8$ ms, respectively. It should be noted that the backlog traffic in each TTI does not only include the newly generated traffic, but also the retransmission traffic, due to the fact that the UEs are allowed to retransmit in the next RTT under the latency constraint. The results have shown that when the latency constraint increases, the backlog traffic in each TTI increases as the retransmission traffic increases. The backlog traffic in each TTI for the Proactive scheme is smaller than that of the K-repetition scheme due to the efficiency of the Proactive scheme, which has been analyzed in details in the following.

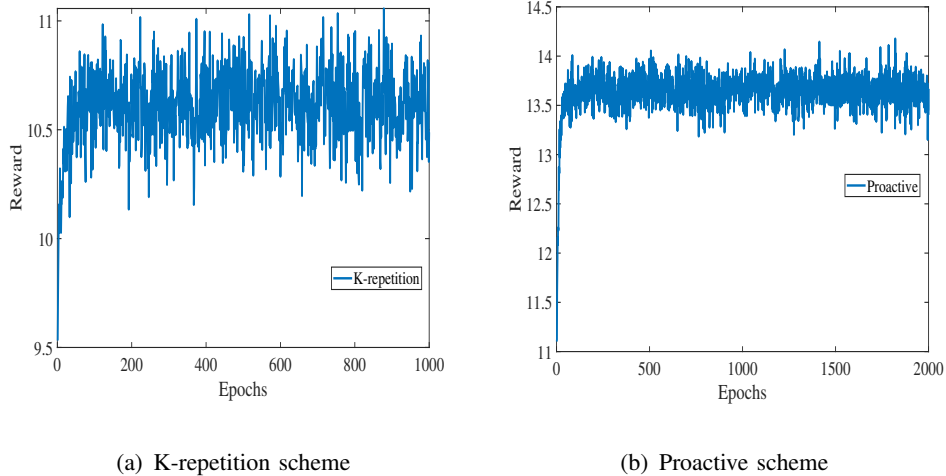


Fig. 11: Average received reward for each GF scheme.

Fig. 11 plots the average received reward for the K-repetition scheme and the Proactive scheme, respectively. It can be seen that the average rewards of both K-repetition and proactive schemes converge to the optimal value after training. We can also observe that the average received reward of proactive scheme in Fig. 11 (b) is higher than that of the K-repetition scheme in Fig. 11 (a). This is because the proactive scheme can terminate the repetition earlier and start new packet transmission with timely ACK feedback, which is able to deal with the traffic more effectively.

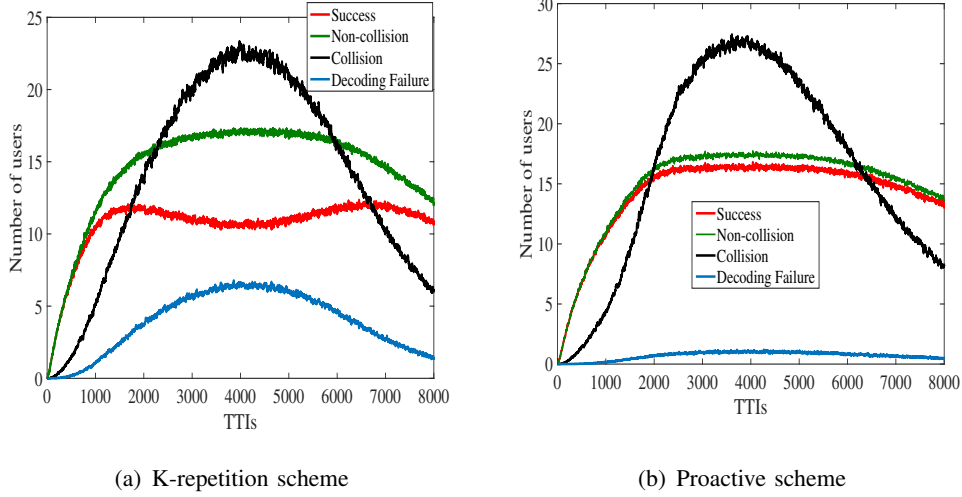


Fig. 12: The transmission results for each GF scheme.

Fig. 12 plots the number of the successfully served UEs, the non-collision UEs, the collision UEs, and the decoding failure UEs for the K-repetition scheme and the Proactive scheme respectively, under latency constraint $T_{\text{cons}} = 2$ ms. It is shown that the number of successfully served UEs achieved under latency constraint for the Proactive scheme is almost up to 1.5 times more than that for the K-repetition scheme. This is due to that the UEs in the Proactive scheme can terminate their repetitions earlier to reduce the interference to other UEs, which leads to an increase in the number of successfully decoding UEs. In both Fig. 12 (a) and Fig. 12 (b), the number of collision UEs has a peak at around the 4000th TTI with the peak traffic at this time as shown in Fig. 10. Due to the fact that only the non-collision UEs can be detected by the UE to decoding their data, the number of successful UEs depends on the number of the non-collision UEs. In addition, the number of failure decoding UEs reaches a peak due to the peak traffic at the 4000th TTI in the K-repetition, which leads to the decrease in the number of successful UEs at that time.

B. Multi-parameter configuration including the repetition values and the CTU number

Fig. 13 plots the average received reward for the K-repetition scheme and the Proactive scheme, respectively, with multi-parameter configuration, including the repetition values and the CTU number. It can be seen that both the average received rewards of the K-repetition and the Proactive scheme converge to an optimal value after training. Compared to Fig. 11 under latency constraint $T_{\text{cons}} = 2$ ms, we observe that the average received reward of two schemes decrease significantly. This is because the larger latency constraint $T_{\text{cons}} = 8$ ms leads to larger retransmission packets, which results in serious traffic congestion. It should be noted that the performance degradation of K-repetition scheme is much larger than that of Proactive scheme, which shows the potential

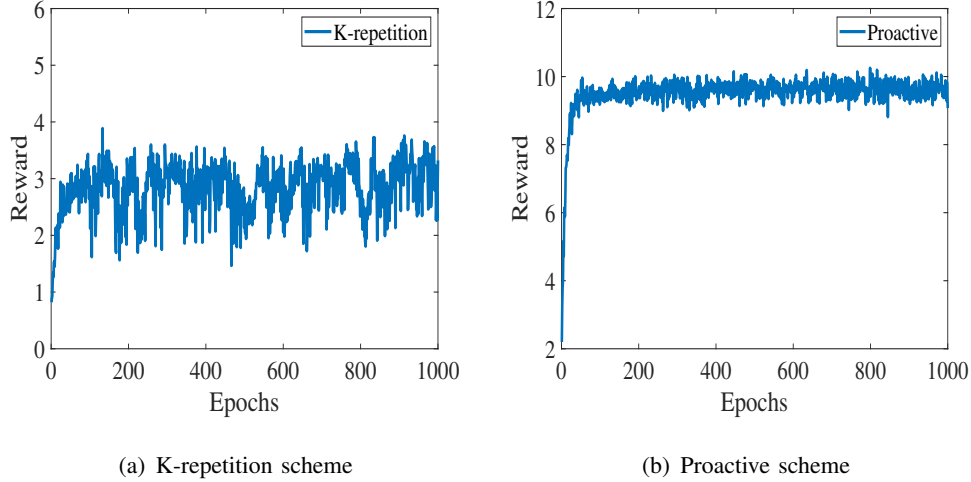


Fig. 13: Average received reward for each GF scheme with multi-parameter configuration.

of the Proactive scheme in heavy traffic and long latency constraint situation due to timely termination.

Fig. 14 plots the number of successful UEs, non-collision UEs, and decoding failure UEs for K-repetition scheme and Proactive scheme, respectively, with multi-parameter configuration including the repetition values and the CTU number under latency constraint $T_{\text{cons}} = 8$ ms. We have observed that the number of non-collision transmission UEs of both scheme is similar. However, the number of decoding failure UEs of the K-repetition scheme is almost up to five times more than that of the Proactive scheme at the peak traffic, due to the interference caused by multiple repetitions from collision UEs, which is consistent with Fig. 15. In addition, it is

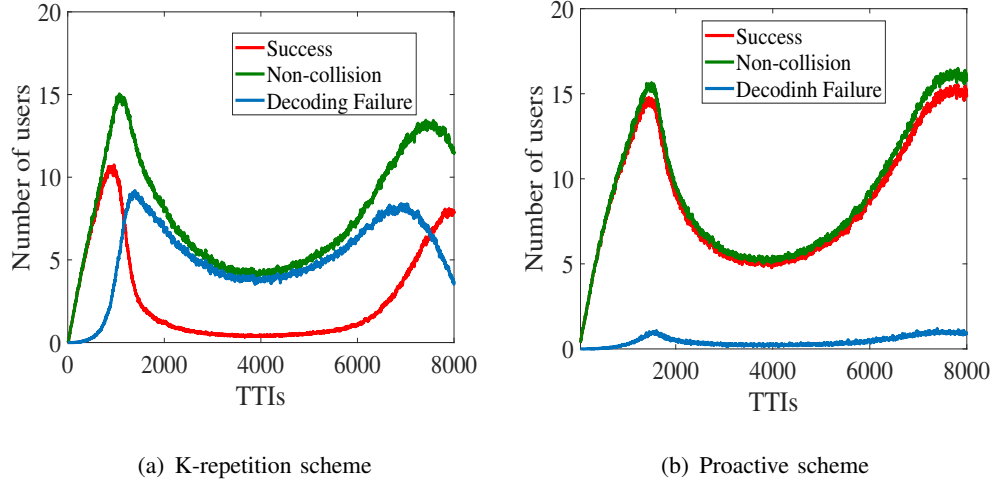


Fig. 14: The transmission results for each GF scheme.

noted that in both the K-repetition scheme and the Proactive scheme, there is lower number of success UEs in high traffic, especially in peak traffic at round 4000th TTI.

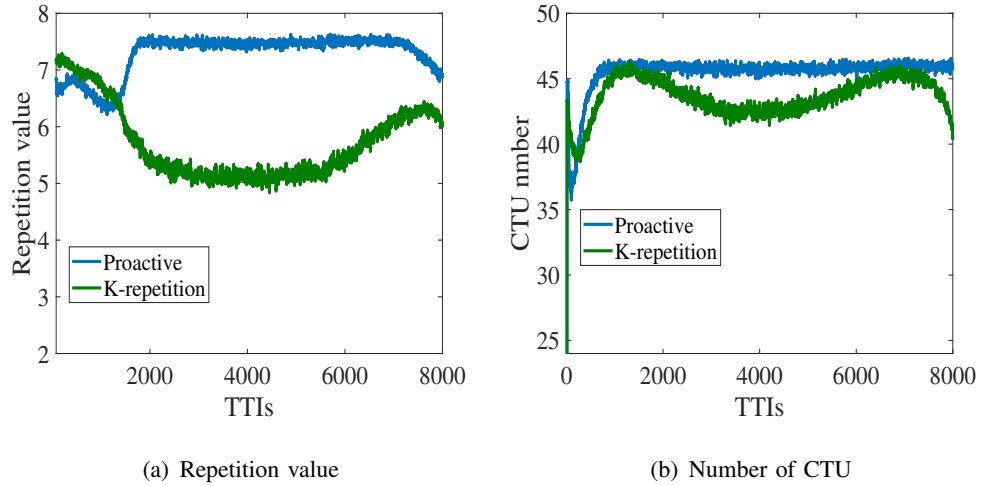


Fig. 15: Actions for each GF scheme.

Fig. 15 plots the actions of each scheme including the repetition value and the number of CTUs for the K-repetition and the Proactive scheme, respectively. In Fig. 15 (a), we can see that the Proactive scheme adopts a higher and more stable repetition value due to its capability to deal with the traffic congestion. However, the repetition value of K-repetition scheme decreases

first and then increases back to a higher value. This is because the agent in K-repetition scheme learns to sacrifice the current successful transmission to alleviate the traffic congestion to obtain a long-term reward. In Fig. 15 (b), It can be seen that the number of CTUs has a similar trend as the repetition value in Fig. 15 (a), which may be caused by the sharing of actions as observations among agents.

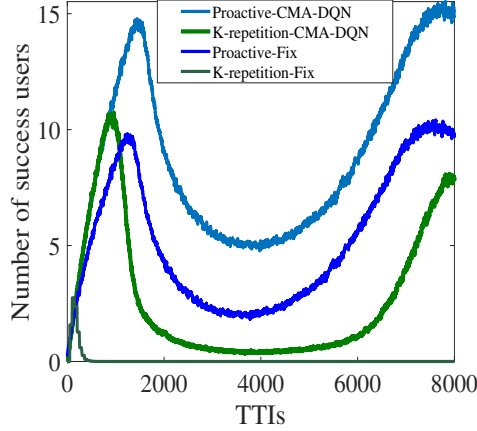


Fig. 16: The average number of success UEs for each scheme with learning framework and fixed parameters.

Fig. 16 plots the average number of success UEs for the K-repetition scheme and the Proactive scheme by comparing that with learning framework and that with fixed parameters, respectively. Here, we set the fixed repetition value $K = 8$ and the CTU number $C = 48$. Our results shown that the number of successfully served UEs achieved under the same latency constraint in our proposed learning framework is up to ten times for the K-repetition scheme, and two times for the Proactive scheme, more than those achieved in the system with fixed repetition values and CTU numbers, respectively. This is because, in the learning framework, the agent learns to dynamically configure lower repetition values and CTU numbers to alleviate the traffic congestion to obtain a long-term reward.

VI. CONCLUSION

In this paper, we developed a general learning framework for dynamic resource configuration optimization in signature-based GF-NOMA systems, including the sparse code multiple access (SCMA), multiuser shared access (MUSA), pattern division multiple access (PDMA), and etc, for

mURLLC services under the K-repetition GF scheme and the Proactive GF scheme. This general learning framework was designed to optimize the number of successfully served UEs under the latency constraint via adaptively configuring the uplink resources, including the repetition values and the contention-transmission unit (CTU) numbers. We first performed a real-time repetition value configuration for the two schemes, where a double Deep Q-Network (DDQN) was developed. We then studied a Cooperative Multi-Agent (CMA) learning technique based on the DQN to optimize the configuration of both the repetition values and the contention-transmission unit (CTU) numbers for these two schemes, by dividing high-dimensional configurations into multiple parallel sub-tasks. Our results have shown that 1) the number of successfully served UEs achieved under the same latency constraint in our proposed learning framework is up to ten times for the K-repetition scheme, and two times for the Proactive scheme, more than those achieved in the system with fixed repetition values and CTU numbers, respectively; 2) with learning optimization, the Proactive scheme always outperforms the K-repetition scheme in terms of the number of successfully served UEs, especially under the long latency constraint; 3) our proposed general learning framework can be used to optimize the resource configuration problems in all the signature-based GF-NOMA schemes; and 4) determining the retransmission or not can be optimized in the future by considering not only the long latency constraint but also the future traffic congestion, due to the fact that long latency constraint will lead to high future traffic congestion.

REFERENCES

- [1] X. Zhang, J. Wang, and H. V. Poor, "Statistical delay and error-rate bounded QoS provisioning for mURLLC over 6G CF M-MIMO mobile networks in the finite blocklength regime," *IEEE J. Sel. Areas Commun.*, pp. 1–1, Sep. 2020.
- [2] W. Saad, M. Bennis, and M. Chen, "A vision of 6G wireless systems: Applications, trends, technologies, and open research problems," *IEEE Network*, vol. 34, no. 3, pp. 134–142, May. 2020.
- [3] "Study on scenarios and requirements for next generation access technologies," *3GPP, TR 38.913 v16.0.0*, Jul. 2020.
- [4] "5G; service requirements for the 5G system," *3GPP, TS 22.261 v17.2.0*, Mar. 2020.
- [5] M. Latva-aho, K. Leppänen, F. Clazzer, and A. Munari, "Key drivers and research challenges for 6g ubiquitous wireless intelligence," 2020.
- [6] "UL grant-free transmission for URLLC," *RI-1705654, 3GPP TSG-RAN WG1 #88*, Apr. 2017.
- [7] N. Ye, H. Han, L. Zhao, and A.-H. Wang, "Uplink nonorthogonal multiple access technologies toward 5G: A survey," *Wireless Commun. Mobile Comput.*, vol. 2018, Jun. 2018.
- [8] T. Taleb and A. Kunz, "Machine type communications in 3GPP networks: potential, challenges, and solutions," *IEEE Commun. Mag.*, vol. 50, no. 3, pp. 178–184, Mar. 2012.
- [9] "Considerations on random resource selection," *RI-1608917, 3GPP TSG RAN WG1 #86*, Oct. 2016.

- [10] “5G; NR; physical layer procedures for data,” *3GPP TS 38.214 v15.9.0*, Mar. 2020.
- [11] “UL grant-free transmission for URLLC,” *R1-1705246*, Apr. 2017.
- [12] “Discussion on HARQ support for URLLC,” *R1-1612246*, *3GPP TR-RAN1 #87*, Nov. 2016.
- [13] “Discussion on explicit HARQ-ACK feedback for configured grant transmission,” *R1-1903079*, *3GPP TSG RAN WG1 #96*, Mar. 2019.
- [14] R. Abbas, M. Shirvanimoghaddam, Y. Li, and B. Vucetic, “A novel analytical framework for massive grant-free NOMA,” *IEEE Trans. Commun.*, vol. 67, no. 3, pp. 2436–2449, Mar. 2019.
- [15] M. B. Shahab, R. Abbas, M. Shirvanimoghaddam, and S. J. Johnson, “Grant-free non-orthogonal multiple access for IoT: A survey,” *IEEE Commun. Surveys Tutorials*, pp. 1–1, May. 2020.
- [16] M. Shirvanimoghaddam, M. Condoluci, M. Dohler, and S. J. Johnson, “On the fundamental limits of random non-orthogonal multiple access in cellular massive iot,” *IEEE J. Sel. Areas Commun.*, vol. 35, no. 10, pp. 2238–2252, Jul. 2017.
- [17] Y. Liu, Y. Deng, N. Jiang, M. ElKashlan, and A. Nallanathan, “Analysis of random access in NB-IoT networks with three coverage enhancement groups: A stochastic geometry approach,” *IEEE Trans. Wireless Commun.*, pp. 1–1, Oct. 2020.
- [18] N. Jiang, Y. Deng, X. Kang, and A. Nallanathan, “Random access analysis for massive IoT networks under a new spatio-temporal model: A stochastic geometry approach,” *IEEE Trans. Commun.*, vol. 66, no. 11, pp. 5788–5803, Jul. 2018.
- [19] Y. Liu, Y. Deng, M. ElKashlan, A. Nallanathan, and G. K. Karagiannidis, “Analyzing grant-free access for URLLC service,” *IEEE J. Sel. Areas Commun.*, pp. 1–1, Aug. 2020.
- [20] J. Zhang, L. Lu, Y. Sun, Y. Chen, J. Liang, J. Liu, H. Yang, S. Xing, Y. Wu, J. Ma, I. B. F. Murias, and F. J. L. Hernando, “PoC of SCMA-based uplink grant-free transmission in UCNC for 5G,” *IEEE J. Sel. Areas Commun.*, vol. 35, no. 6, pp. 1353–1362, Jun. 2017.
- [21] X. Dai, Z. Zhang, B. Bai, S. Chen, and S. Sun, “Pattern division multiple access: A new multiple access technology for 5G,” *IEEE Wireless Commun.*, vol. 25, no. 2, pp. 54–60, Apr. 2018.
- [22] Z. Yuan, C. Yan, Y. Yuan, and W. Li, “Blind multiple user detection for grant-free MUSA without reference signal,” in *2017 IEEE 86th Veh. Technol. Conf. (VTC-Fall)*, Sep. 2017, pp. 1–5.
- [23] C. Wei, H. Liu, Z. Zhang, J. Dang, and L. Wu, “Approximate message passing-based joint user activity and data detection for NOMA,” *IEEE Commun. Lett.*, vol. 21, no. 3, pp. 640–643, Mar. 2017.
- [24] B. Wang, L. Dai, T. Mir, and Z. Wang, “Joint user activity and data detection based on structured compressive sensing for NOMA,” *IEEE Commun. Lett.*, vol. 20, no. 7, pp. 1473–1476, Jul. 2016.
- [25] A. T. Abebe and C. G. Kang, “Comprehensive grant-free random access for massive low latency communication,” in *2017 IEEE Int. Conf. Commun. (ICC)*, Jul. 2017, pp. 1–6.
- [26] N. Ye, X. Li, H. Yu, A. Wang, W. Liu, and X. Hou, “Deep learning aided grant-free NOMA toward reliable low-latency access in tactile internet of things,” *IEEE Trans. Ind. Infor.*, vol. 15, no. 5, pp. 2995–3005, Jan. 2019.
- [27] N. Ye, X. Li, H. Yu, L. Zhao, W. Liu, and X. Hou, “DeepNOMA: A unified framework for NOMA using deep multi-task learning,” *IEEE Trans. Wireless Commun.*, vol. 19, no. 4, pp. 2208–2225, Jan. 2020.
- [28] W. Kim, Y. Ahn, and B. Shim, “Deep neural network-based active user detection for grant-free NOMA systems,” *IEEE Trans. Commun.*, vol. 68, no. 4, pp. 2143–2155, Jan. 2020.
- [29] “Cellular system support for ultra-low complexity and low throughput Internet of Things (CIoT),” *3GPP, Sophia Antipolis, France, TR 45.820 V13.1.0*, Nov. 2015.
- [30] “Study on RAN improvements for machine-type communications,” *3GPP, TR 37.868 v11.0.0*, Sep. 2011.
- [31] “Solutions for collisions of MA signatures,” *R1-1608860*, *3GPP TSG-RAN WG1 #86*, Oct. 2016.
- [32] “On MA resource and MA signature configurations,” *R1-1609227*, *3GPP TSG-RAN WG1 #86*, Oct. 2016.

- [33] J. Navarro-Ortiz, P. Romero-Diaz, S. Sendra, P. Ameigeiras, J. J. Ramos-Munoz, and J. M. Lopez-Soler, "A survey on 5G usage scenarios and traffic models," *IEEE Commun. Surveys Tutorials*, vol. 22, no. 2, pp. 905–929, Feb. 2020.
- [34] A. K. Gupta and S. Nadarajah, *Handbook of beta distribution and its applications*. CRC press, 2004.
- [35] "Study on physical layer enhancements for NR ultra-reliable and low latency case (URLLC)," *3GPP, TR 38.824 v16.0.0*, Mar. 2019.
- [36] K. Au, L. Zhang, H. Nikopour, E. Yi, A. Bayesteh, U. Vilaipornsawai, J. Ma, and P. Zhu, "Uplink contention based SCMA for 5G radio access," in *2014 IEEE Globecom Workshops (GC Wkshps)*, Dec. 2014, pp. 900–905.
- [37] A. C. Cirik, N. M. Balasubramanya, L. Lampe, G. Vos, and S. Bennett, "Toward the standardization of grant-free operation and the associated NOMA strategies in 3GPP," *IEEE Commun. Standards Mag.*, vol. 3, no. 4, pp. 60–66, Dec. 2019.
- [38] Y. Chen, A. Bayesteh, Y. Wu, B. Ren, S. Kang, S. Sun, Q. Xiong, C. Qian, B. Yu, Z. Ding, S. Wang, S. Han, X. Hou, H. Lin, R. Visoz, and R. Razavi, "Toward the standardization of non-orthogonal multiple access for next generation wireless networks," *IEEE Commun. Mag.*, vol. 56, no. 3, pp. 19–27, Mar. 2018.
- [39] R. S. Sutton and A. G. Barto, *Reinforcement learning: An introduction*. MIT press, 2018.
- [40] V. Mnih, K. Kavukcuoglu, D. Silver, A. A. Rusu, J. Veness, M. G. Bellemare, A. Graves, M. Riedmiller, A. K. Fidjeland, G. Ostrovski *et al.*, "Human-level control through deep reinforcement learning," *nature*, vol. 518, no. 7540, pp. 529–533, 2015.
- [41] H. Van Hasselt, A. Guez, and D. Silver, "Deep reinforcement learning with double q-learning," *arXiv preprint arXiv:1509.06461*, Dec. 2015.
- [42] T. Tieleman and G. Hinton, "Lecture 6.5-rmsprop: Divide the gradient by a running average of its recent magnitude," *COURSERA: Neural Netw. Mach. Learn.*, vol. 4, no. 2, pp. 26–31, Oct. 2012.
- [43] "Study on new radio access technology-physical layer aspects," *3GPP, TR 38.802 v14.0.0*, Mar. 2017.